JGR Oceans

RESEARCH ARTICLE
10.1029/2019JC015613

Eddy-Driven Cross-Shelf Transport in the East Australian Current Separation Zone

Neil Malan[1,2], Matthew Archer[1], Moninya Roughan[1,2], Paulina Cetina-Heredia[1,2], Michael Hemming[1,2], Carlos Rocha[1,2], Amandine Schaeffer[1,2], Iain Suthers[3,4], and Eduardo Queiroz[1,2]

[1]School of Mathematics and Statistics, University of New South Wales, Sydney, New South Wales, Australia, [2]Centre for Marine Science and Innovation, University of New South Wales, Sydney, New South Wales, Australia, [3]Sydney Institute of Marine Science, Mosman, New South Wales, Australia, [4]School of Biological Earth and Environmental Sciences, University of New South Wales, Sydney, New South Wales, Australia

Key Points:
- An eddy dipole mode is the main driver of cross-shelf transport in the East Australian Current extension
- Dipole events can result in onshore velocities up to 1.78 m s^{-1}, with a maximum transport at 33–34°S
- Water from the observed dipole jet is advected from offshore up to the midshelf in the form of a warm salty intrusion of offshore water

Supporting Information:
- Supporting Information S1

Correspondence to:
N. Malan,
neilcmalan@gmail.com

Citation:
Malan, N., Archer, M., Roughan, M., Cetina-Heredia, P., Hemming, M., Rocha, C., et al. (2020). Eddy-driven cross-shelf transport in the East Australian Current separation zone. *Journal of Geophysical Research: Oceans*, *125*, e2019JC015613. https://doi.org/10.1029/2019JC015613

Received 2 SEP 2019
Accepted 21 JAN 2020
Accepted article online 20 FEB 2020

Abstract In western boundary current systems, sharp velocity gradients between the poleward flowing jet and coastal waters generally act to inhibit cross-shelf exchange. Downstream of jet separation, dynamic mesoscale eddies dominate the flow. In the East Australian Current System, counter-rotating eddy dipoles are often present which, in the appropriate configuration, have potential to drive cross-shelf transport. However, this eddy dipole mode is poorly understood in the framework of cross-shelf exchange and the effect of these structures on shelf waters is uncertain. Using 25 years of satellite altimetry, as well as in situ sampling of a typical dipole event, we investigate the characteristics of eddy-driven cross-shelf exchange. We show that the maximum onshore velocity is driven by an eddy dipole structure and occurs in a defined latitudinal band between 33°S and 34°S more than 50% of the time. We sample a typical eddy dipole and find a strong onshore jet, 37 km wide, with velocities up to 1.78 m s^{-1} and a transport of at least 16 Sv. Hydrographic data from an autonomous underwater glider show that this jet manifests on the shelf as a subsurface intrusion of warm salty water extending from offshore up onto the midshelf. In the light of climatic changes in western boundary current transport and the increase in their eddy kinetic energy, understanding eddy-driven cross-shelf exchange is important to predict future changes to the shelf water mass.

1. Introduction

The East Australian Current (EAC) completes the western branch of the south Pacific subtropical gyre, carrying warm water poleward along the east Australian coast. It has its source in the South Equatorial Current, which splits into a series on jets (including the South Caledonia Jet), before feeding into the EAC (Figure 1). Between 30°S and 32°S, the EAC usually separates from the coast (Cetina-Heredia et al., 2014), splitting into the eddy-dominated southern and eastern extensions (Oke et al., 2019). At the separation point, anticyclonic eddies are shed approximately every 100 days via a mixed baroclinic/barotropic instability mechanism (Bowen et al., 2005; Bull et al., 2017; Mata et al., 2006).

Cross-shelf exchange dominates the pathways by which nutrients and biological and other materials enter and leave shelf systems. This is due to the strong cross-shelf gradients in temperature, salinity, and dissolved material between the shelf and the deep ocean, thus implying that exchange of water between deep ocean and shelf results in mixing of vastly different water masses. This means that cross-shelf flows, which tend to be of a far smaller magnitude than their along-shelf counterparts, can have an impact of on shelf water properties which far outweighs their relatively small magnitudes (Brink, 2016). A key feature of the inshore edge of western boundary currents is the strong horizontal current shear and thus steep vorticity gradients between the energetic core of the current and the more quiescent coastal and shelf waters. These sharp gradients between the deep ocean and coastal waters act as a barrier to inhibit water mass and properties exchanges (Harrison & Siegel, 2014; Roughan et al., 2011). The momentum balance across the shelf is largely in geostrophic equilibrium, driven by pressure gradients set by the western boundary current (Roughan et al., 2003; Schaeffer et al., 2013). Episodic exchanges have been documented, driven predominantly by wind stress (e.g., Fewings et al., 2008), bottom stress (Schaeffer et al., 2014), or frontal instabilities (He et al.,

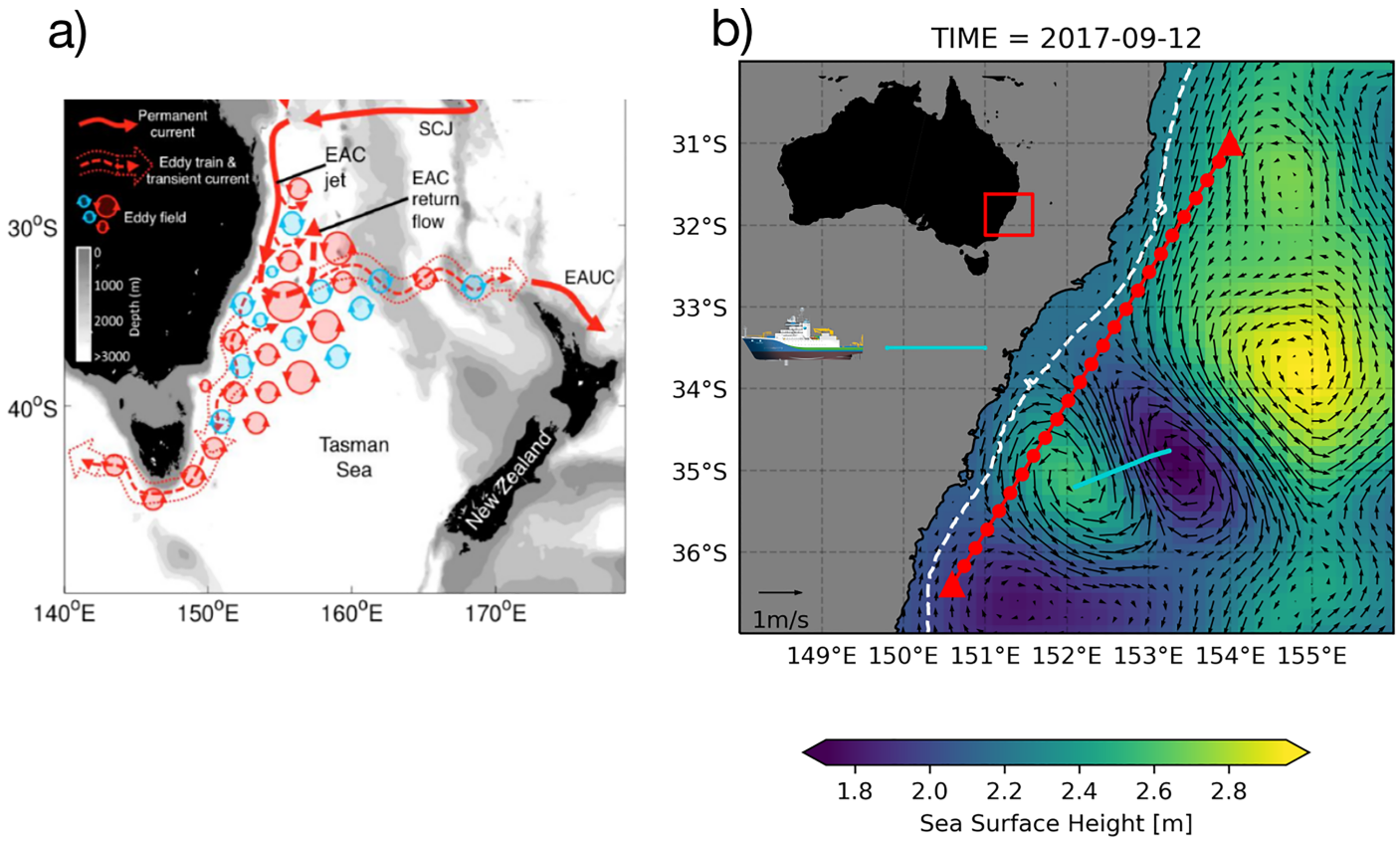

Figure 1. Map showing (a) location and schematic view of EAC separation and extension region (adapted from ; Oke et al., 2019) and (b) the location of the shelf section (red dots) overlaid on a snapshot of satellite sea surface height and geostrophic currents from 12 September 2017. The 200 m isobath is plotted in white, and the track of the research vessel across the dipole is shown in blue.

2018; Schaeffer et al., 2017) but are usually restricted to periods of less than 10 days, resulting in productivity being inhibited by a lack of retention in the shelf system (Everett et al., 2014; Olson, 2001).

While there is some similarity between the structure of the main jet across the major western boundary currents (Archer et al., 2018), after these jets separate from the coast, these similarities appear to end. The Gulf Stream and Kuroshio are both bounded on the poleward side by cold, fresh, equatorward flowing currents as part of the subpolar gyre (Tomczak & Godfrey, 2003), while the Agulhas Current overshoots the southern tip of the African continent and retroflects back toward the east in the open ocean (Beal et al., 2011; Lutjeharms, 2006). The South Brazil Current ends in a turbulent eddy field as it collides with the Malvinas Current to form the Brazil-Malvinas confluence (Gordon, 1989; Peterson & Stramma, 1991). The EAC does not interact with any other strong current after its separation from the coast, resulting in a unique mesoscale eddy field. The EAC is notable among the western boundary currents, as it has a weaker transport and main jet, but eddy kinetic energy of the same order as the larger western boundary systems (i.e., Agulhas, Gulf Stream, and Kuroshio) (Pilo et al., 2015; Rykova et al., 2017). In the EAC extension, the anticyclones are of a similar depth and strength to the Kuroshio and Gulf Stream anticyclones, while the cyclonic eddies are markedly weaker with less isopycnal displacement than any of the other western boundary current systems (Rykova et al., 2017).

Despite these different regimes, across the Western Boundary Current systems, the first eddying mode of variability often plays a first-order role in facilitating cross-shelf exchange by acting to break down the relative vorticity barrier of the main current jet (e.g., Malan et al., 2018; Ryan et al., 1999; Vélez-Belchí et al., 2013; Zhang & Gawarkiewicz, 2015). The EAC sheds eddies all along its latitudinal range (Cetina-Heredia, Roughan, Sebille, et al., 2019; Oke et al., 2019), but more consistently around 32°S in the separation zone, when the jet extends poleward, sheds an eddy, and then rapidly retracts northward (Bull et al., 2017; Cetina-Heredia et al., 2014; Godfrey et al., 1980). Downstream of the EAC separation zone (Cetina-Heredia

et al., 2014; Ribbe & Brieva, 2016), the flow becomes eddy dominated (Everett et al., 2015), with productivity increasing almost linearly with latitude (Everett et al., 2014). This increased productivity has been attributed to the increase in eddy activity poleward of the EAC, with Everett et al. (2012) focusing on the increase in chlorophyll-A in cyclonic eddies in the so-called "Eddy Avenue." These eddies have been shown to be productive (Roughan et al., 2017), as well has having the ability to retain water as they are advected with the background flow (Cetina-Heredia, Roughan, Liggins, et al., 2019). However, whether eddies can deliver water onto the shelf remains an open question.

The process of interaction between cyclonic and anticyclonic eddies, in the form of the creation of a counter-rotating eddy dipole structure, is particularly interesting, since these interactions can change eddy properties and shape (Cresswell & Legeckis, 1986; Pallàs-Sanz & Viúdez, 2007). This change in shape could be important for the transport of heat, salt, and biological material in light of the effect which eddy eccentricity has on the retention or leakage of water within these eddies (Pilo et al., 2018). Eddies that elongate tend to leak water, while eddies that remain circular retain more of their water (Cetina-Heredia, Roughan, Sebille, et al., 2019). Persistent eddy structures can be key for larval dispersal (Cetina-Heredia, Roughan, Liggins, et al., 2019) and are important to understand, as they are unstable modes and so could be more sensitive to changes in the energy dynamics of a western boundary system than the main current jet itself.

In this paper we investigate the role of eddy dipole structures in cross-shelf transport in the eddy-dominated EAC extension. The dipole structure is investigated using both satellite and in situ observations to show both its ubiquity and impact on the shelf.

2. Data and Methods

2.1. Satellite Altimetry

We use the satellite altimetry product distributed by the Integrated Marine Observing System (accessed at portal.aodn.org.au), which merges satellite altimetry with sea level elevation measurements from coastal tide gauges (Deng et al., 2011). Spatial resolution is 0.2°. The sea level anomalies as well as the absolute dynamic topography and their derived geostrophic currents are used in our analysis. This data set was used to assess the latitudinal variability of mesoscale cross-shelf velocities across a section of the shelf edge from 31°S, 154°E to 36.4°S, 150.6°E (red transect in Figure 1b). From here on this is referred to as the shelf section. The geostrophic velocities derived from altimetry are linearly interpolated onto this section and rotated 27° in order to lie normal to the shelf break; we consider this cross-shelf component of the geostrophic velocity field to be an approximation of the mesoscale cross-shelf flow.

Spatial patterns of variability are extracted from the sea level anomalies using empirical orthogonal functions, calculated using the methods and routines provided by Dawson (2016). Backward-in-time Finite-size Lyaponov exponents (FSLE) are derived from daily geostrophic velocities and provided by AVISO at a spatial resolution of 0.04°. Here they are used to show the spatial extent of the dipole jet and upwelling front, as FSLE ridges approximate Lagrangian Coherent structures such as filaments and fronts (Beron-Vera et al., 2009) and have been shown to be robust against random noise mimicking unresolved scales (Cotte et al., 2011). Following the method outlined in d'Ovidio et al. (2004), the AVISO product calculates the exponential rate of separation of seeded particles (λ) during an advection time (t). This is defined as $\lambda = t^{-1}\log(\frac{\delta_0}{\delta_f})$. $\delta_0 = 0.02°$, $\delta_f = 0.6°$, and a maximum time integration of 200 days which approximates the mesoscale.

2.2. Structures Driving Cross-Shelf Exchange

When considering the effect of mesoscale eddy structures on the shelf circulation, and especially cross-shelf exchange, it is instructive to separate out dominant patterns of eddying variability which consistently impact the shelf. However, ranking the importance of various spatial patterns of eddies can be difficult, due to the inherent range of eddy configurations and rotation directions possible. Here, to simplify the analysis, the eddies are considered solely through the lens of their role in driving cross-shelf velocity, thus meaning that the patterns identified are the eddy structures which most strongly affect cross-shelf exchange.

To do this, latitude of maximum cross-shelf transport along the shelf section is identified for each day of the altimetry era, from 1993 to 2018, using the cross-shelf geostrophic velocities from the shelf section. The resulting distributions of both latitude of maximum cross-shelf velocity and the strength of those cross-shelf velocities are shown in Figure 2. All onshore values greater than the median value (0.25 m s^{-1}

westward/onshore) are considered cross-shelf exchange events, allowing a composite mean of cross-shelf exchange events to be constructed (Figure 3).

2.3. Shipboard Observations

An archetypal eddy dipole located directly downstream of the EAC separation point was sampled in September 2017. In situ measurements were made from the R/V Investigator during a research cruise (https://doi.org/10.4225/08/5a964b9041903) operated by the Australian Marine National Facility. In this study we analyze measurements of near-surface temperature, vertical profiles of horizontal velocity, near-surface wind, and the trajectories of ten 15 m drogued Surface Velocity Program (SVP) drifters from NOAA (https://doi.org/10.25921/7ntx-z961), released within the eddy dipole. The near-surface temperature was recorded onboard the ship by a thermosalinograph with an intake depth of 7.9 m (Sea-Bird-SBE 21). Wind speed and direction during the dipole transect were measured with a wind vane on the starboard (upwind) mast (RM Young Wind Sensor Type 05108). A shipboard acoustic Doppler current profiler (SADCP), operating at 75 kHz in narrowband mode, measured vertical profiles of the horizontal currents beneath the ship. The measurement range was approximately 800 m with 8 m vertical bin spacing and a sampling interval of 5 min resulting in a horizontal resolution of approximately 1,200 m in the transect used here. The top good velocity bin was obtained at a depth of approximately 30 m. SADCP data were quality controlled by Marine National Facility staff using the University of Hawaii's Common Ocean Data Access System. A Triaxus (a vertically profiling towed body) was deployed to map the hydrographic structure of the dipole in high resolution. It carries a dual-sensor Seabird SBE 911, collecting temperature, conductivity, pressure, and dissolved oxygen. The Triaxus was towed at a speed of 8 knots ($\sim$ 4 m s^{-1}), approximately 1.5 km behind the vessel, in a sawtooth pattern with horizontal spacing of $\sim$2 km over vertical dives of $\sim$200 m.

The 10 drifters were deployed along the dipole jet transect, in five locations. At each location, we deployed two SVP drifters. In this paper, we show analysis of drifter trajectories from 12 September 2017 to 14 September 2017, the time period over which the drifters were initially within the eddy dipole. The location of the SVP drifters is measured every 10 min (at hour output), and speeds are calculated from these positions using the Haversine method to calculate distance per hour.

2.4. Glider Observations

During the study period, as part of the regular monitoring line maintained by the New South Wales Integrated Marine Observing System with support from the Australian National Glider Facility (ANFOG), a Slocum autonomous glider was deployed from Forster at approximately 32°S. The glider performed a zigzag transect pattern along the shelf as it was carried poleward by the EAC. Data from this deployment are used between the 16 and 24 September 2017 when it transited the productive area of wide ($\sim$80 km in from shore to 1,000 m isobath) shelf between 32.5°S and 34°S, known as the Stockton Bight. The glider carried a pumped Seabird CTD (conductivity-temperature-depth; sampling frequency 0.2–0.8 Hz). Historical data from two previous Slocum glider missions in the Stockton Bight in the same month (20–30 September 2010 and 1–10 September 2016, data on the shelf and between 32.7°S and 33.2°S) are also used.

3. Results

3.1. The Presence of a Dipole Mode in the EAC Extension

A latitude-time Hovmoller plot of the cross-shelf geostrophic velocities along the shelf section (Figure 2a) reveals onshore flow between 33°S and 34°S, in contrast to the offshore flow which dominates the rest of the domain. A time mean of the cross-shelf geostrophic velocities from 1993–2018 (Figure 2b) shows that the flow is onshore in the mean only between 33°S and 34°S. The peak time mean value of cross-shelf velocity in this area of onshore flow is 0.1 m s^{-1} at 33.5°S, while the highest offshore time mean velocity occurs north of 32°S with values approaching 0.2 m s^{-1}. The distribution of these offshore velocities can be seen binned by latitude in Figure 2c, with maximum offshore velocities occurring most frequently between 31°S and 32°S, presumably due to the separation of the main part of the EAC jet, and a second peak at $\sim$35°S in the very south of the domain.

On more than 50% (5,148 out of 9,308) of the days from 1993–2018, the maximum daily onshore velocity along a section from 31°S to 36°S occurs in a zone between 33°S and 34°S, with a secondary peak near 36°S. (see Figure 2d). The distribution of these values of daily maximum onshore velocity is skewed to the left, with a median value of $\sim$ 0.25 m s^{-1} (Figure 2e). Dipole eddy structures persist on timescales of weeks to up to 2 months. The periodicity of the cross-shelf flow averaged between 33°S and 34°S (both on and offshore) is

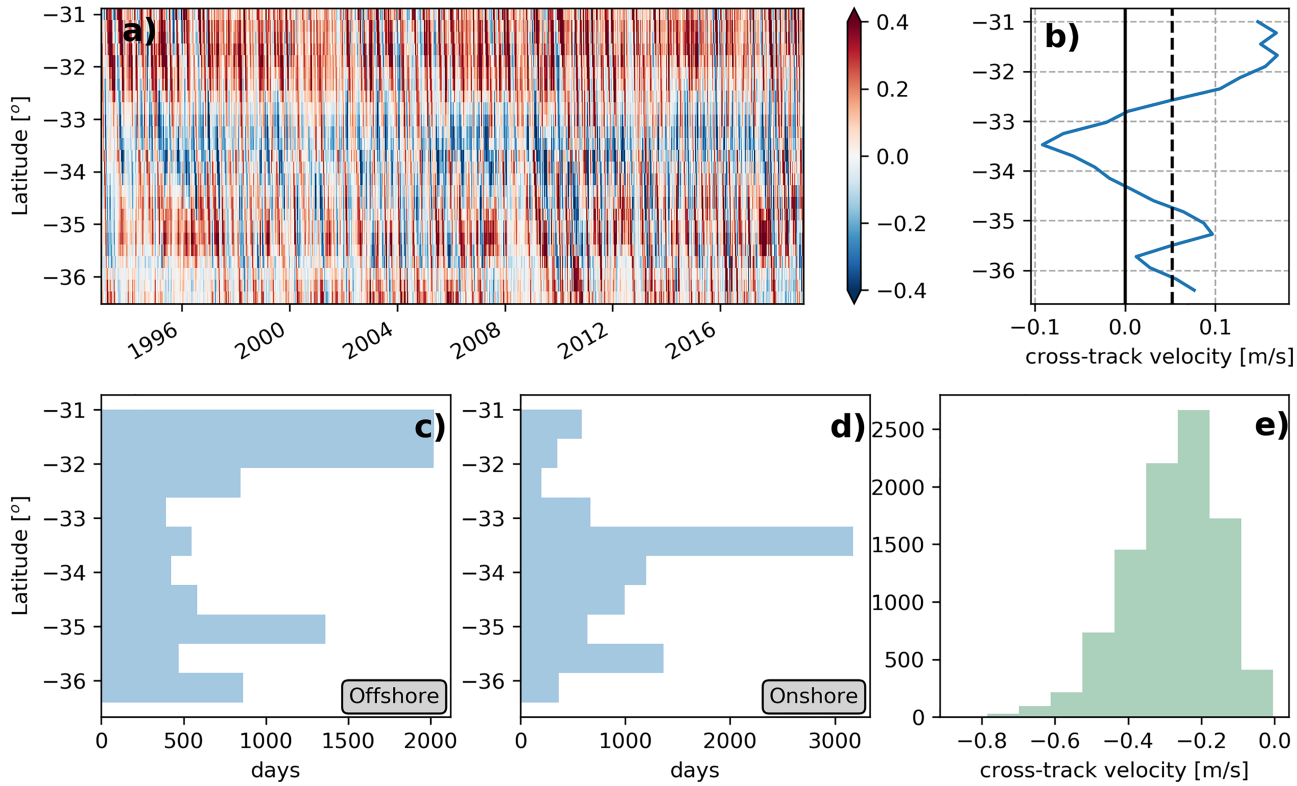

Figure 2. (a) Hovmoller plot of cross-shelf velocity along the shelf section, (b) time-mean of cross-shelf velocities from 1993–2018 (mean value shown as vertical dashed black line), (c) latitude distribution of maximum offshore velocity, (d) latitude distribution of daily maximum onshore velocity, and (e) distribution of velocity values at that maximum (negative values indicate onshore flow).

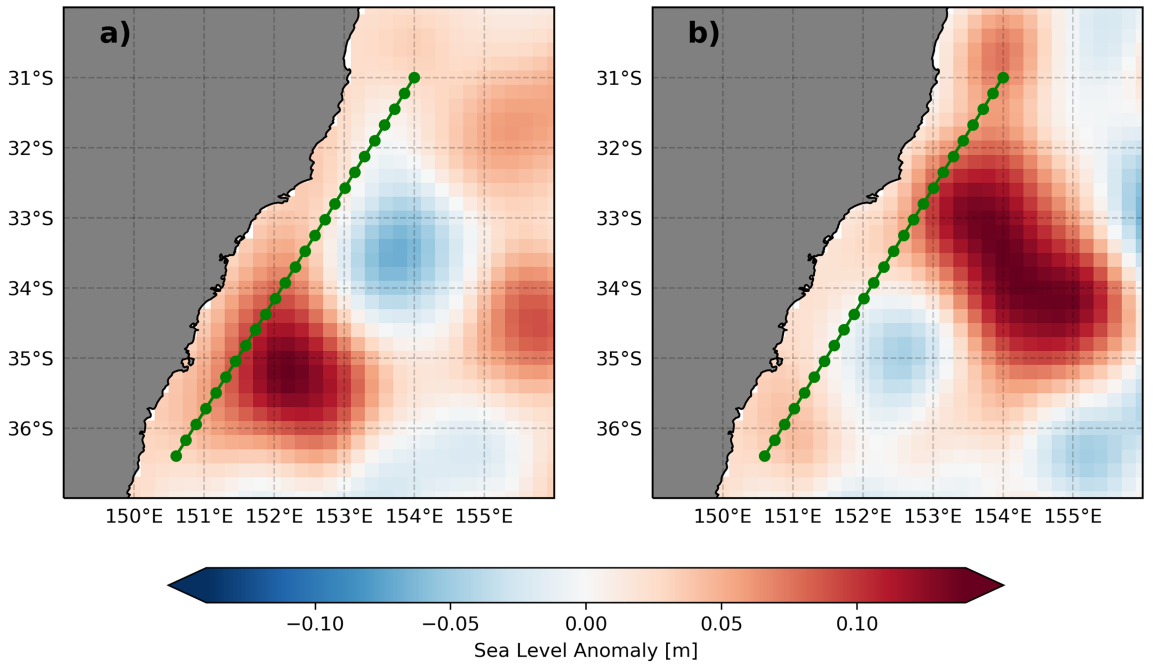

Figure 3. Composite mean of sea level anomalies for (a) strong onshore transport events and (b) weak onshore transport events. Strong onshore transport events are defined by maximum onshore velocities being 0.25 m s^{-1} or more. The shelf section is marked in green.

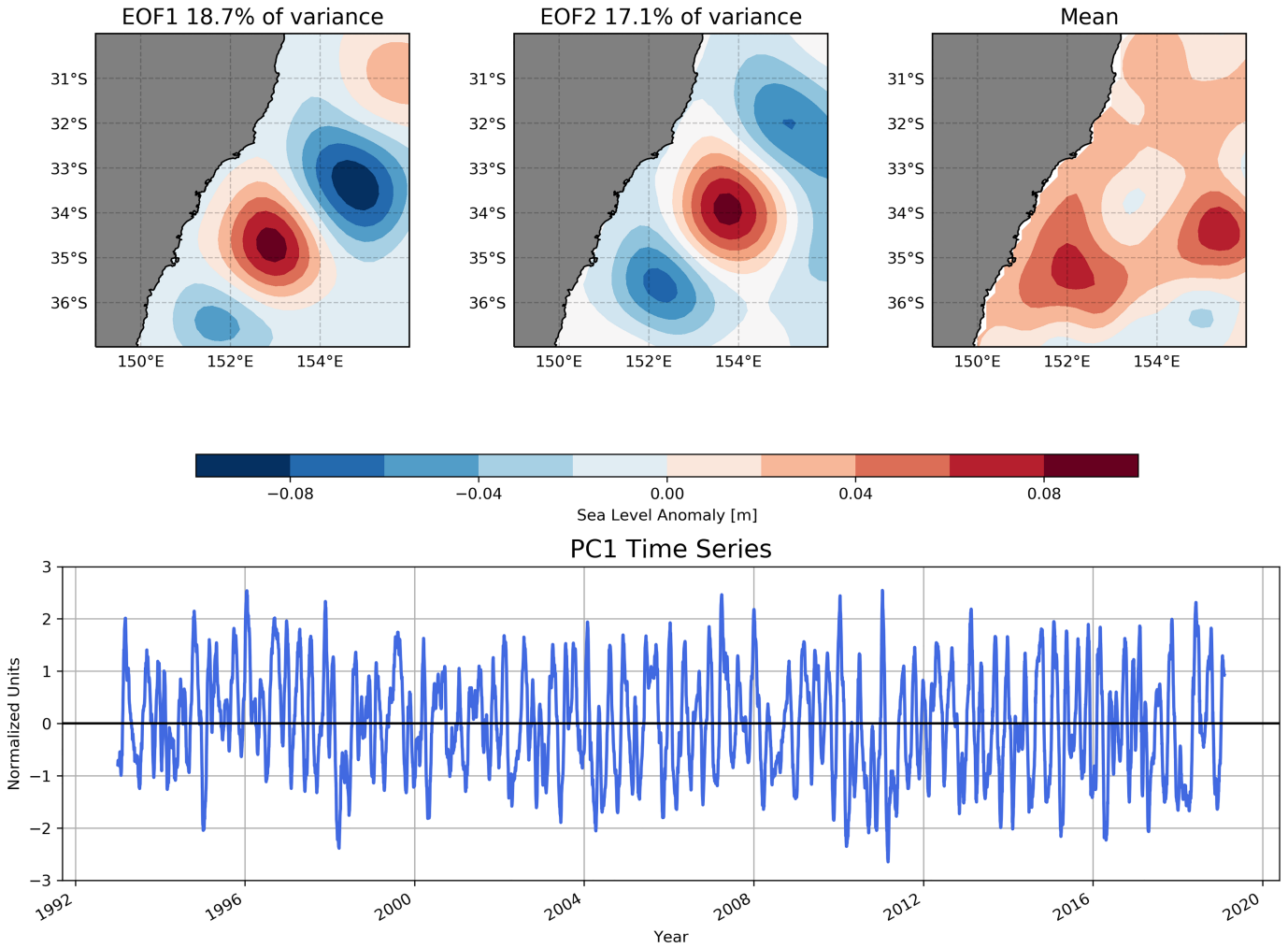

Figure 4. The two leading empirical orthogonal functions of satellite-derived sea level anomaly, as well as the time-mean, calculated from 1993–2018 (top) and the time series of the principle component representing the first EOF mode of sea level anomaly (bottom).

examined by way of a spectral analysis (supporting information Figure S1), which shows a strong periodicity around the 90–130 day EAC eddy-shedding timescale (Bowen et al., 2005).

A composite mean of days with greater than median onshore velocity (i.e., >0.25 m s^{-1} toward the coast) anywhere along the shelf section, shows these events of strong onshore geostrophic velocities to occur during the presence of an eddy dipole structure (Figure 3a). The eddy dipole manifests in the composite mean (Figure 3a) as a circular minimum in sea level anomaly, corresponding to a cyclonic eddy, lying just offshore of the shelf break, centered at 33.5°S, 153.7°E. Directly to the south west of this is a circular maximum in sea level anomaly centered at 35.2°S, 152.2°E. Both structures are approximately 200 km in diameter and thus similar in size and shape to mesoscale eddies. The composite mean of days with onshore transport weaker than the median (Figure 3b) shows a less eddy like pattern with an oblong maximum in sea level anomaly, associated with anticyclonic circulation, extending offshore in a south easterly direction from the coast at 32°S.

To complement the composite analysis, the eddying variability of the system was examined using empirical orthogonal functions (EOF) of sea level anomaly (Figure 4). The first EOF mode (Figure 4a), which explains 18.7% of the variance, exhibits the same dipole structure as the composite mean of strong cross-shelf velocity events shown in Figure 3a. The second EOF of sea level anomaly (Figure 4b), explaining 17.1% of the variance, shows a different configuration of eddy-like structures, with a weaker minimum in the north of the domain and the maximum in the middle of the domain positioned farther north than in the first EOF. The mean sea level anomaly (Figure 4c) shows the ubiquity of strong eddy-like patterns between 34°S and

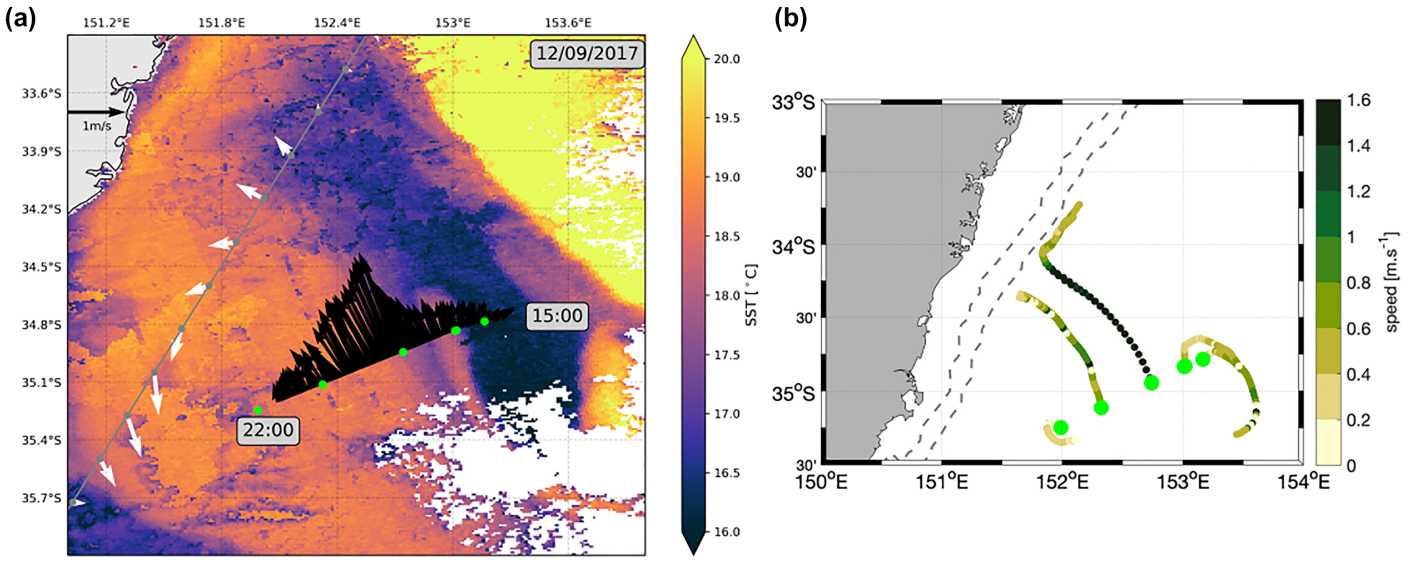

Figure 5. (left) Ship track showing SADCP transect, ADCP measured velocities at 30 m depth (black vectors) and drifter deployment locations (green dots). Gray line indicates the shelf section transect and the altimetrically derived geostrophic velocities (white vectors). All are overlaid over MODIS sea surface temperature. (right) Tracks of the deployed drifter pairs over the first 48 hr of their deployment, colored by speed. Deployment locations are shown in bright green, and the dashed gray contours show the 200 and 1,000 m isobaths.

36°S. The time series of the principle component representing the first EOF mode (Figure 4d) correlates significantly with the time series of cross-shelf velocities averaged between 33°S and 34°S, with $r = 0.55$ ($p = 0.001$). Interestingly, the second EOF shows an eddy-like structure farther south at the bottom of the domain with its associated onshore or offshore flow positioned near 36°S, corresponding to the latitude of the secondary peak of onshore velocity seen in Figure 2c.

3.2. Dipole Case Study

The cruise transect sampled during the eddy dipole event in September 2017 enabled the nature of these dipole structures to be examined in more detail. The transport of the jet produced by the counter-rotating eddies was quantified by way of a quasi-synoptic SADCP transect which was undertaken between eddy centers between 15:00 and 22:00 on 12 September 2017 (Figure 5a). The interaction of the two counter-rotating mesoscale eddies resulted in a strong surface jet with cross-transect velocities of up to 1.78 m s^{-1}, oriented to the northwest. This corresponded to geostrophic velocities across the shelf section of 0.4 m s^{-1} (Figure 5a), putting it within the range of common cross-shelf velocities in the altimetry record (Figure 2e). The error in shipboard ADCP measurements can be up to 0.05 m s^{-1} (Beal et al., 2008). Along the 120 km long transect between the eddy centers, velocities are stronger on the anticyclonic eddy (southwest) side of the transect and increase steadily to peak approximately halfway between the eddy centers. From the halfway point between the eddy centers, the velocity drops off sharply (to <1 m s^{-1}) on the cyclonic side of the dipole. (Figure 5a).

The core of the jet, defined as where velocities are over 1 m s^{-1}, is 37 km wide and extends down to a depth of 200 m. Velocities greater than 0.5 m s^{-1} extend down to 600 m (Figure 6). While surface velocities in the core of the jet are stronger on the anticyclonic side of the dipole, velocities at depth are more symmetrical (Figure 6). Transport across the transect, calculated by extrapolating the topmost velocity value (at 30 m depth) to the surface and then vertically integrating down to the 800 m extent of the SADCP velocity measurements, is estimated to be 16 Sv.

The tracks of the SVP drifters enable the examination of the advection driven by this dipole jet over time. The drifters were deployed in pairs along the SADCP transect between the eddy centers (see green dots in Figure 5 for locations). The pair deployed near the high-velocity center of the dipole (at ~35°S 152.8°E (from here on referred to as the "core pair") continues to advect rapidly (at over 1.4 m s^{-1}) toward the shelf, with both drifters reaching the shelf break within 48 hr of deployment. On reaching the shelf edge, both drifters in the core pair abruptly turn 90° and head northeast along the edge of the shelf (Figure 5b). The temperature sensors aboard the drifters also show a drop in sea surface temperature from 18.5 to 17 °C at the time of

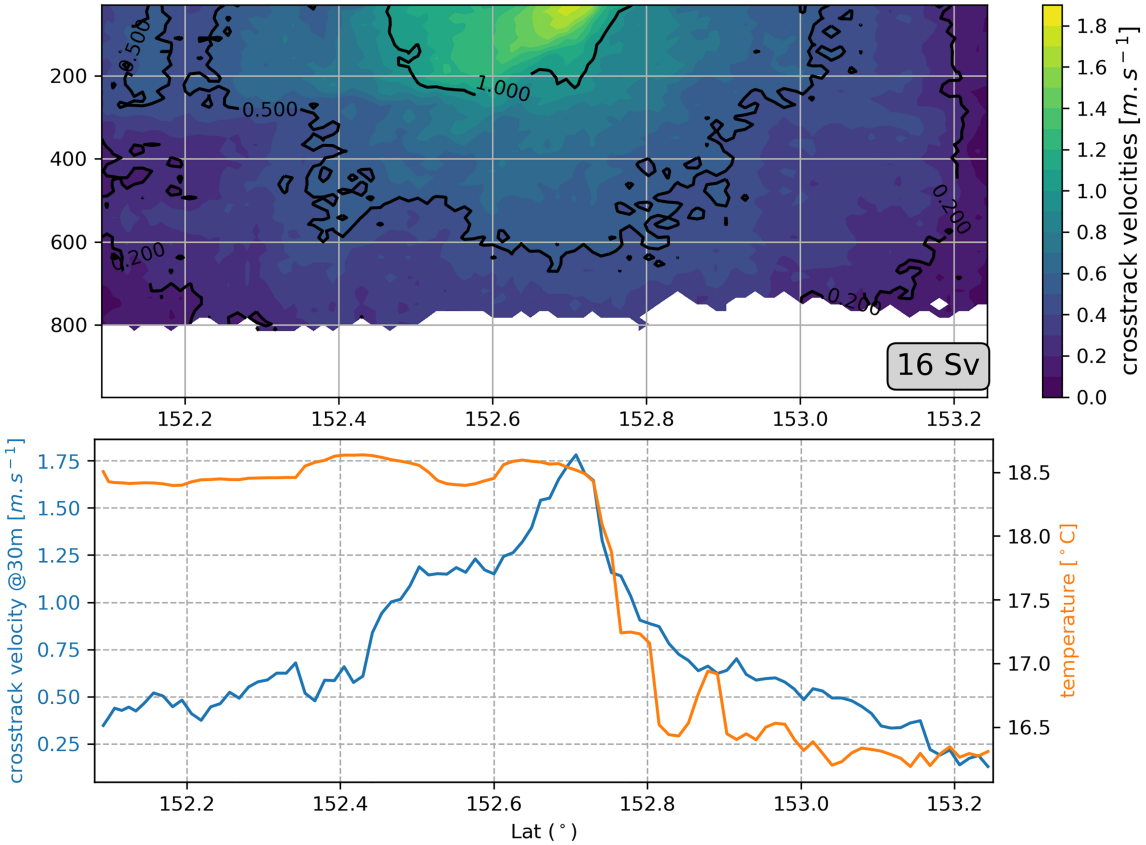

Figure 6. Top: Shipboard ADCP section across dipole with 1, 0.5, and 0.2 m s^{-1} velocity contours highlighted. Bottom: Surface currents and temperature from ship's underway system. Temperature is taken at approximately 7.9 m, while currents are measured at 30 m.

this direction change. This drop in temperature is consistent with the sea surface temperature gradient seen where the cold core cyclonic eddy interacts with the shelf water in the satellite image in Figure 5a. Interestingly, this north eastward flow is not present in the geostrophic velocities (e.g., in Figure 1b) indicating that the front is too small in scale and close to the coast to be resolved by altimetry. The next closest drifter pair to the jet (the "secondary pair"), while deployed to the southwest of the core pair in lower velocities of 1 m s^{-1}, also heads directly toward the shelf break, but due to advecting more slowly, does not reach it in the first 48 hr. However, in the next 12 hr (see animation in supporting information), both drifters in the secondary pair perform a similar 90° turn to that of the core pair, although this time to head southwest, rather than north east, along the shelf break.

The drifter pairs deployed on each edge of the transect follow the flow of their respective mesoscale eddies, looping clockwise (anticlockwise) in the cyclonic (anticyclonic) flow. There was little separation between the drifters of each pair during this initial 48 hr period, indicative of large-scale stirring by the mesoscale eddy field as the dominant process (Beron-Vera et al., 2009), as opposed to a situation where smaller-scale processes are dominant, acting on the drifters to separate them. It is important to note that throughout the drifter deployment, the wind blew steadily from the north at 5–10 m s^{-1} and thus provided favorable conditions for coastal upwelling. This coastal upwelling would result in divergence at the coast, inhibiting the flow of surface water from the open ocean to the shelf and forming an SST front at the shelf break, as evidenced by the sudden change of direction and drop in temperature experienced by the drifter pair deployed closest to the center of the dipole.

3.3. Impact of the Dipole on the Shelf

The spatial patterns of the sampled eddy dipole are shown in terms of SST, ocean color, and Lagrangian structures (via FSLE; Figure 7). As expected cool SSTs are encountered in the cyclonic side of the dipole and warm SSTs on the anticyclonic eddy side of the dipole. However, these thermal footprints extend farther

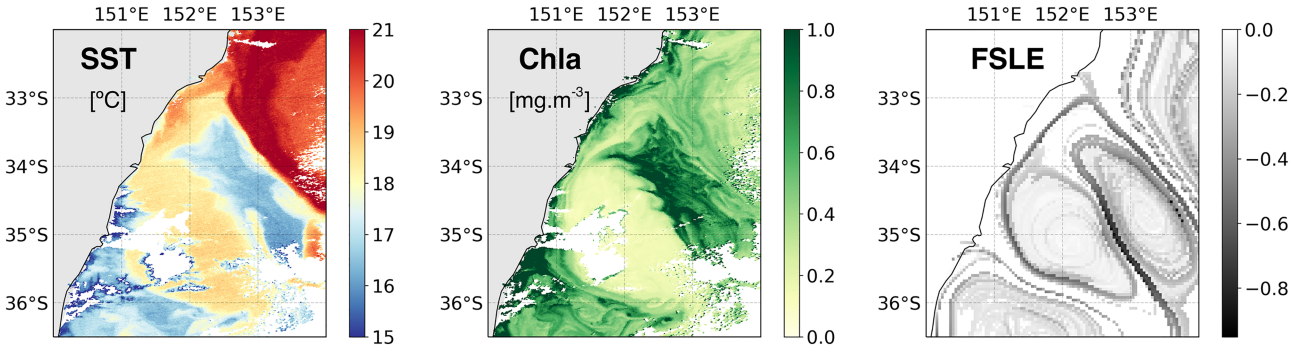

Figure 7. The 3 day composite of satellite-derived sea surface temperature from MODIS, chlorophyll concentration from MODIS, and finite-size Lyapanov Exponents calculated from altimetry during the dipole event on 13 September 2017.

onto the shelf than would be expected from the size of the eddies when viewed using sea surface height (Figure 1).

The satellite-derived surface observations of chlorophyll show high concentrations in the cyclonic eddy extending toward the shelf (Figure 7). Although not the subject of this study, it is interesting to note the clear submesoscale wave-like pattern superimposed onto the larger-scale dipole structure. These small instabilities occur along the edge of the area of high productivity, visible in both the SST and chlorophyll images and lying along a strong ridge in FSLE. Along the coast, there is a clear break between the high productivity along the coast and the high productivity in the cyclonic eddy. The FSLE ridges also show evidence of this separation between the shelf waters and the mesoscale eddy dynamics offshore between 33°S and 33.5°S. However, over the next 12 days, this pattern evolves; from the 16 to 18 September, the high chlorophyll water is advected closer to the shelf, from the 19 to 21 September, it begins to move southwestward (downstream) along the coast, and by 22 to 24 September appears to have been advected onto the shelf (Figure 8a). Chlorophyll concentrations have increased inshore of 33.2°S, 152°E, and the offshore water is no longer clearly separated from the coastal area of high productivity (Figure 8b). This merging of offshore water with the coastal front is also visible in the evolution of the FSLE structures over time.

Hydrographic observations along the shelf obtained from the glider from 16 to 24 September 2017 show the continuous presence of high chlorophyll water out to the edge of the shelf break (Figure 8b). This captures the linking of the coastal and offshore chlorophyll maxima observed over time in the satellite imagery. At the offshore edge of each glider transect, the glider begins to interact with offshore water from the dipole jet. This interaction is marked by a deepening of the chlorophyll maximum and an increase in both temperature (Figure 8c) and salinity (Figure 8d). This increase in temperature and salinity is most apparent at the offshore end of the transect on 20 September (marked by the vertical dashed red line on Figure 8). Here the temperature at a depth of 100 m increased by 2 °C and the salinity increased from 35.5 to over 35.7 psu. An increase in chlorophyll is also observed at this depth. This intrusion of warm salty water at depth appears as a round bolus in the glider time series in Figure 8, as the glider makes a turn and returns back up the shelf, sampling the same feature twice. On the next long offshore transect (22 and 23 September) the glider again samples this warm and salty intrusion at depth and shows it to be present from midshelf to the shelf break, as the glider samples all the way out to the 200 m isobath. The depth of the intrusion is ~50 m at the shelf break and 100 m midshelf.

To confirm whether the warm and salty intrusion of water onto the shelf was anomalous and whether it originated in the dipole, the temperature-salinity characteristics of both the shelf and the eddy dipole jet are compared (Figure 9). The temperature-salinity (T-S) characteristics of the glider mission during the dipole were compared to two previous September glider missions (2010 and 2016). Additionally, the T-S of the gliders was also compared to that of the CSIRO Atlas of Regional Seas (CARS) (Ridgway et al., 2002) for the month of September on the shelf (<200 m depth) in the same latitudinal range as the glider missions. To show the T-S of the core of the dipole jet, we select the temperature and salinity profiles taken by the Triaxus within the 1 m s^{-1} velocity contour (i.e., between 152.5°S and 152.8°S on 6), with a depth range sampled of 50–250 m. We found that during the dipole event, the shelf was >0.1 psu saltier than both glider and CARS climatology (Figure 9a). This increase in salinity is particularly apparent between 50 and 100 m of depth,

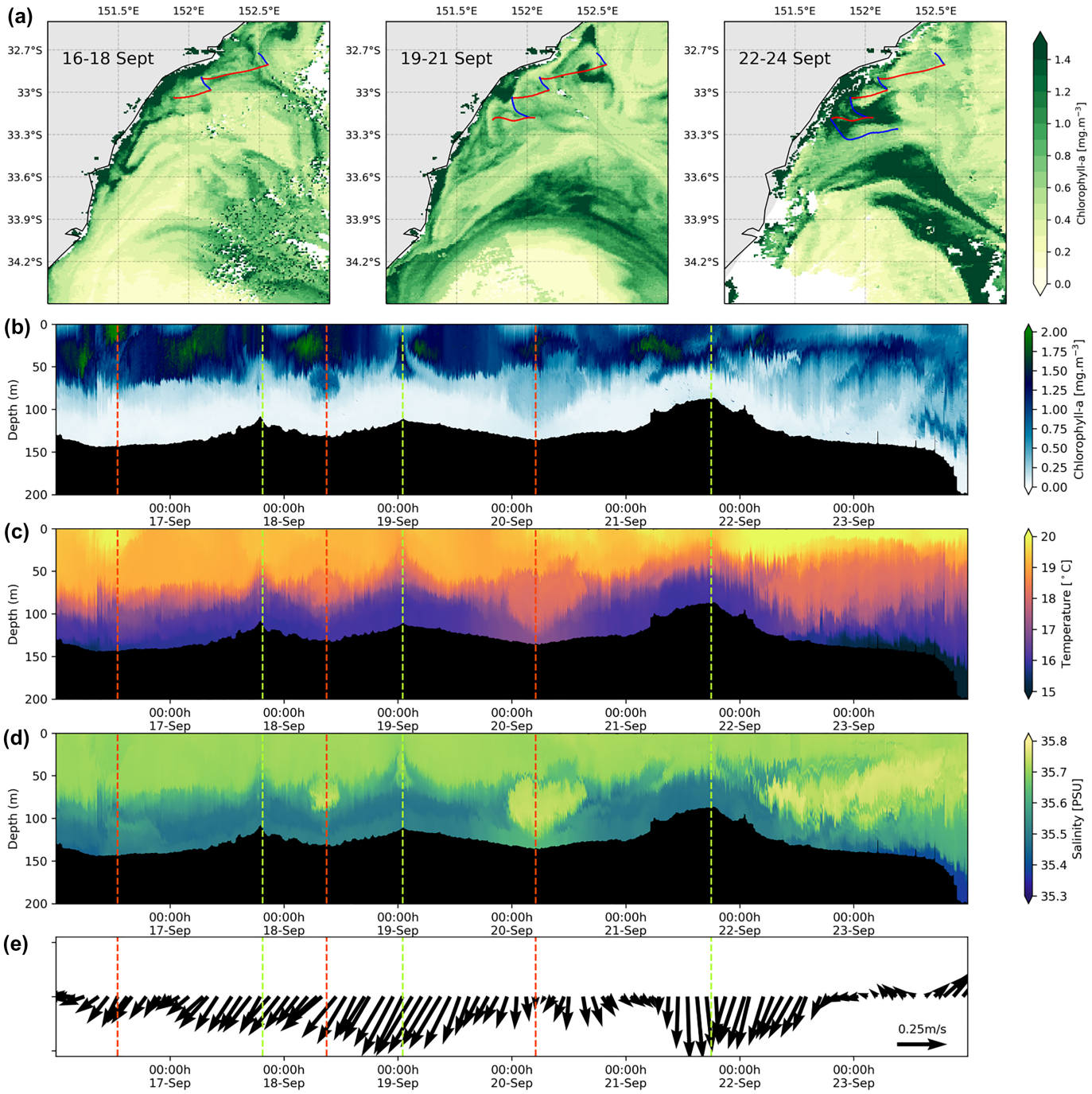

Figure 8. (a) The 3 day composites of MODIS chlorophyll from 16–24 September 2017. Glider track is marked in blue (offshore transect) and red (onshore transect). Rest of figure: time series of (b) chlorophyll, (c) temperature, (d) salinity, and (e) hourly depth-averaged currents from a Slocum glider mission during the dipole event. The vertical red dashed lines show the offshore end of the glider transects, while the vertical green dashed lines show the inshore ends.

with surface water also being 0.5 °C warmer and saltier than the climatological mean. The water sampled by the Triaxus offshore in the jet between the two eddies exhibited the same high salinity characteristics as the saltiest shelf water, indicating that the wide range of salinity observed on the shelf at the time of the dipole is most likely due to mixing between the colder, fresher shelf water, and the warmer saltier dipole jet water. This mixing is best illustrated in terms of spice, shown in Figure 9b, which shows the difference between the shelf water, represented by the historical gliders and CARS, and the spicier (warmer and saltier) dipole jet water sampled offshore by the Triaxus. Thus, the intrusion of offshore water driven by the eddy dipole

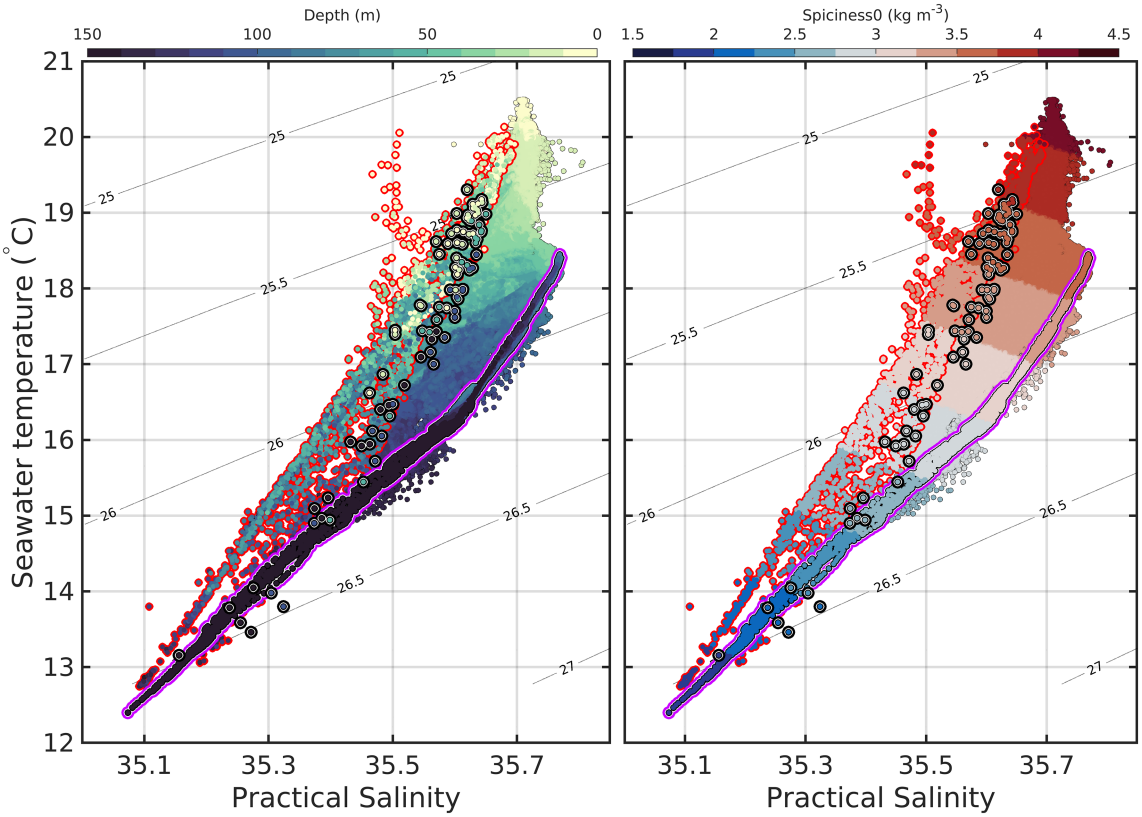

Figure 9. Temperature-salinity colored by depth (left) and spice (right) obtained from the Slocum glider mission during the dipole event. Overlaid are temperature-salinity data from the CARS climatology (black circles), previous September glider missions (red circles), and shipboard Triaxus measurements taken offshore in the center of the dipole jet (outlined in magenta).

has increased the gradient of spice on the shelf. The water intruded onto the shelf by the dipole jet, although coming from the core of the jet, is more reminiscent of anticyclonic side of the dipole. This appears linked to the asymmetry in velocity between the two eddy centers, with velocities on the anticyclonic side of the dipole jet being almost double those on the cyclonic side. Thus, the dipole jet is made up of more water from the anticyclonic eddy than from the cyclonic eddy (see Figure 5a) due to the anticyclonic eddy being more energetic, which is a general pattern in the EAC (Rykova et al., 2017).

Of course, warm salty water can also be brought onto the shelf from the north by an EAC intrusion event. However, an examination of the depth-averaged currents from the glider mission during the sampled dipole event (Figure 8e) shows this not to be the case. Depth-averaged currents on the shelf (sampled from the 17 to 22 September) are predominately toward the southwest (U and V components both negative). From 22 September, when the glider enters the main body of the intrusion of the dipole jet (Figure 8d), the current shifts from flowing southerly at 0.2 m s^{-1} to flow to the northeast and then northwest at 0.1 m s^{-1} on 23 September. Generally, the areas of shelf not associated with the intrusion (e.g., on 19 September) have strong southwestward flow, while where we see salinity maximums associated with the intrusion (e.g., in the early hours of 20 and 22 September onward), the current slows down and ultimately turns northward (Figure 8e). Thus, the intrusion of warm salty water has come from the south, that is, the dipole jet, rather than from the EAC itself in the north.

4. Discussion and Summary

4.1. Cross-Shelf Transport

An examination of the cross-shelf velocities across a section defined along the shelf edge in the EAC separation zone shows that, upstream of 32.5°S and downstream of 34°S, the cross-shelf geostrophic velocities follow the accepted idea of being offshore in the mean. However, this is not the case between 33°S and 34°S, where we have showed that the cross-shelf geostrophic flow is onshore in the mean. This generally onshore flow occurs just downstream of the latitude at which the EAC most commonly separates from the coast

(Cetina-Heredia et al., 2014). The composite analysis of days with strong (greater than median) onshore transport reveals an eddy dipole pattern as the main driver of onshore transport at 33–34°S. A spectral analysis performed on the time series of onshore flow between these two latitudes (supporting information Figure S1) shows a strong peak at a periodicity centered at 100 days. This 100-day periodicity is consistent with the eddy-shedding timescale at the EAC separation, as shown by Mata et al. (2006) and confirmed by Cetina-Heredia et al. (2014) and Bull et al. (2017). Therefore, it follows that the strong onshore velocities are driven by eddy dipoles associated with the regular shedding of anticyclonic eddies from the EAC in the separation zone. These eddy dipoles are quasi-stationary, with residence times ranging from weeks to months. This is in contrast to frontal eddies, smaller cyclonic features that form on the inshore edge of the EAC, which have been previously shown to drive cross-shelf transport (e.g., Roughan et al., 2017; Schaeffer et al., 2017). A systematic quantification of the formation and duration of frontal eddies (Schaeffer et al., 2017) showed that they are far more ephemeral in time, as they translate down the shelf and so do not lead to an increase in the retention of productive water on the shelf.

4.2. Cross-Shelf Transport Confined to Specific Latitudes

From the analysis of cross-shelf transport we have shown that strong onshore transport occurs dominantly within a single degree of latitude (between 33°S and 34°S) and secondarily at 36°S. This localization is contrary to the immediate idea of onshore transport being driven by an eddy dipole which then propagates poleward down "Eddy Avenue" as one would assume from Everett et al. (2012). If this were the case, then the onshore transport would be more evenly distributed between 33°S and 36°S. However, our results have showed that this is not the case, with the onshore flow associated with the eddy dipole more focused at a specific latitude. So why do the dipoles not propagate poleward along the shelf? Cetina-Heredia, Roughan, Liggins, et al. (2019), using eddy tracking techniques, find that while anticyclonic eddies move in a corridor along the southeast coast of Australia, as is expected from the literature, the cyclonic eddies tend to follow a more zonal path translating to the west. In fact, using model output from the Ocean Forecast for the Earth Simulator with (1/10)° resolution, Cetina-Heredia, Roughan, Liggins, et al. (2019) found only three cyclones over a 2 year period to transit the zone poleward along the shelf between 34°S and 38°S. Many more cyclones are diagnosed north of 33°S and across the Tasman Sea (their Figure 4). The predominant translation direction of cyclones is to the west. These differing propagation directions between cyclones and anticyclones may also explain the "gap" in the eddy field between 35°S and 38°S which is seen in Pilo et al. (2015) (their Figure 7a), who use the eddy data set from Chelton et al. (2007) to examine eddy properties in Southern Hemisphere western boundary currents. From examination of individual dipole events from satellite altimetry, it seems that often the cyclonic eddy forms during the shedding of the anticyclonic eddy from the EAC, which sets up a large horizontal shear field between the north branch of the eddy (flow onshore) and the EAC flowing offshore to the east. It is possible that without this shear from the EAC itself, the cyclonic eddy, and thus the dipole, dissipates without propagating farther south. This essentially forms a quasi-steady location for the dipole feature, thus ensuring that the onshore transport is located between 33°S and 34°S and prevents the cross-shelf transport from being more evenly distributed along the southeast Australian coast. Exceptions to this rule (like the three cyclones observed by Cetina-Heredia, Roughan, Liggins, et al. (2019)) appear to take place when the EAC remains attached to the coast and could be responsible for the small secondary peak in onshore flow observed at 36°S. To our knowledge, these "crossroads" of cyclonic and anticyclonic eddies have not previously been described and merit their own dedicated study.

4.3. Description of a Dipole-Driven Onshore Jet

The dipole-driven jet observed by the RV Investigator during September 2017 is most notable for its intense currents, strong horizontal shear, and large onshore transport of 16 Sv. Put into context, the transport of the dipole jet is more than half of the poleward transport of the EAC at 27°S, where it is most coherent (Sloyan et al., 2016). Due to the limited depth of the SADCP transect (only the upper 800 m of the water column was measured) used to calculate the transport, and all measured values being positive in the onshore direction, this 16 Sv number is likely to be an underestimation. Additionally, this is not one of the stronger onshore transport events in the altimetry era (Figure 2), meaning that there may be unobserved dipole jets with still greater transport. More importantly, the main component of this transport is onshore, and glider observations during the time of the dipole show a clear signature of offshore water being advected all the way up to the midshelf. This advection occurs despite the upwelling favoring winds during the sampled dipole event also creating a situation where the warm, salty water of the dipole jet appears to have subducted beneath the warm surface upwelling front at the shelf edge (Figures 8c and 8d, note that the intrusion water

has the same T-S characteristics as the dipole jet water sampled by the Triaxus). The upwelling front also manifests as a ridge of FSLE indicating surface convergence parallel to shore in Figure 7; in agreement with this pattern, the surface drifters (Figure 5b) were advected up and down shelf along this upwelling front. It follows that this inflow to the shelf and subsequent bifurcation equatorward (with the cyclonic eddy) and poleward (with the anticyclonic eddy) will result in outflows to the north and south of the dipole. This outflow of shelf water to the north of an eddy dipole has been previously observed and is discussed (in terms of an independent event rather than being identified as part of the recurrent eddy dipole structure) by Baird et al. (2008).

4.4. Biological Implications and Mixing

The observed dipole event shows elevated chlorophyll values offshore which, over a 2 week period, advects toward the coast, and merges with the coastally driven productivity on the shelf. The presence of the strong dipole-driven jet, which is shown to advect water onto the midshelf, provides a plausible mechanism for the delivery of larvae and other biological material from the deep ocean to the midshelf. Although in the sampled dipole event the transport onto the shelf took place in the subsurface layers, it could be hypothesized that downwelling, rather than upwelling winds, would result in transport onto the shelf in the surface layers as well. Additionally, the interaction of two mesoscale eddies in a dipole could cause them both to change shape, increase their eccentricity, and leak water as suggested by Cetina-Heredia, Roughan, Liggins, et al. (2019). Our results support the idea of eddy interaction and changes in shape leading to water leakage, with satellite imagery showing productive water from inside the cyclonic eddy leaking into the dipole jet and being advected onto the shelf. It is possible that the quasi-stationary characteristic eddy dipole results in them having greater biological significance, acting as a "larval superhighway" to reliably deliver biologically active material from offshore to a specific part of the coastline. Due to their ubiquity, these dipole-driven cross-shelf exchange events may also have a strong impact on retention and residence times of shelf water and contribute to mixing by bringing spicier water onto the shelf, resulting in increased interleaving between water masses.

4.5. Climate Change Impacts

Under a changing climate, the EAC has been shown to be strengthening, as well as warming at two to three times the global average (Wu et al., 2012). Cetina-Heredia et al. (2014) have shown this to manifest in the EAC as an increase in eddy-driven transport and a poleward trend in the EAC separation latitude. As the eddy dipole structure explored in this paper appears to rely on the intersection between the zonal tracks of cyclonic eddies and the meridional tracks of anticyclonic eddies, we hypothesize that it may be particularly sensitive to changes in the structure and distribution of eddies in the EAC system. A change in eddy properties could result in perturbation of the dipoles driving cross-shelf exchange in this region. A freshening of EAC eddies has already been observed (Rykova & Oke, 2015), and the eddy kinetic energy of the EAC is projected to increase and penetrate farther poleward in a changing climate (Oliver et al., 2015). Quantifying the impact these changes could have on eddy-driven cross-shelf exchange requires an increased understanding and modeling capability of ageostrophic motions (such as the dipole jet) resulting from eddy-eddy interactions, as highlighted recently on a global scale by Zhang et al. (2019).

4.6. Conclusion

Onshore geostrophic velocities in the EAC separation zone are focused in a specific latitudinal band between 33°S and 34°S. Composite and EOF analyses show these cross-shelf velocity events, which can have geostrophic currents speeds of up to 0.7 m s^{-1}, are driven by an eddy dipole mode that creates a cross-shelf jet. In situ observations of an archetypal eddy dipole jet show it to extend over 800 m in depth, with strong surface velocities (up to 1.78 m s^{-1}) and an onshore transport of 16 Sv. Temperature and salinity sampled by an autonomous underwater glider show that this dipole jet pushes warm salty water all the way to the midshelf, possibly increasing mixing between shelf and offshore water masses and increasing the lateral gradient of spiciness in the shelf waters.

Our results provide a mechanism for the maximum in larval transport immediately downstream of the EAC separation shown by the Lagrangian modeling results of Cetina-Heredia, Roughan, Sebille, et al. (2019) and so could have an implication for the distribution of free floating particles, both biologically active and inert, along the southeast Australian coast. Western boundary currents are already showing significant climate change impacts with eddy-driven transport increasing in recent years; hence, understanding the role of

eddy-driven cross-shelf exchange, as well as particle dispersion in the mesoscale, is important in light of projected changes to the EAC transport and eddy field under future climate.

Acknowledgments
The authors would like to thank the captain, crew, and collaborators aboard RV Investigator voyage IN2017 V04 "The whole enchilada." Cruise data can be found online (https://www.cmar.csiro.au/data/trawler/). Drifter data form part of the Global Drifter Program and can be found online (https://www.aoml.noaa.gov/phod/gdp/interpolated/data/subset.php). FSLE are distributed by Aviso (https://www.aviso.altimetry.fr/). All other data used in this study can be found at the Australian Ocean Data Network portal (https://portal.aodn.org.au/). IMOS is supported by the Australian Government through the National Collaborative Research Infrastructure Strategy and the Super Science Initiative. This work was partially funded by Australian Research Council Linkage Grant ARC LP150100064 to MR. PCH and CR were partially funded by LP150100064. IS acknowledges funding from ARC Discovery grant DP150102656.

References

Archer, M. R., Keating, S. R., Roughan, M., Johns, W. E., Lumpkin, R., Beron-Vera, F. J., & Shay, L. K. (2018). The kinematic similarity of two western boundary currents revealed by sustained high-resolution observations. *Geophysical Research Letters*, *45*, 6176–6185. https://doi.org/10.1029/2018GL078429

Baird, M. E., Timko, P. G., Middleton, J. H., Mullaney, T. J., Cox, D. R., & Suthers, I. M. (2008). Biological properties across the Tasman Front off southeast Australia. *Deep Sea Research Part I: Oceanographic Research Papers*, *55*(11), 1438–1455. hppts://doi.org/10.1016/J.DSR.2008.06.011

Beal, L. M., De Ruijter, W. P. M., Biastoch, A., & Zahn, R. (2011). On the role of the Agulhas system in ocean circulation and climate. *Nature*, *472*(7344), 429–436. hppts://doi.org/10.1038/nature09983

Beal, L. M., Hummon, J. M., Williams, E., Brown, O. B., Baringer, W., & Kearns, E. J. (2008). Five years of Florida Current structure and transport from the Royal Caribbean Cruise Ship Explorer of the Seas. *Journal of Geophysical Research*, *113*, 1–11. hppts://doi.org/10.1029/2007JC004154

Beron-Vera, F. J., Olascoaga, M. J., Beron-Vera, F. J., & Olascoaga, M. J. (2009). An assessment of the importance of chaotic stirring and turbulent mixing on the West Florida Shelf. *Journal of Physical Oceanography*, *39*(7), 1743–1755. hppts://doi.org/10.1175/2009JPO4046.1

Bowen, M. M., Wilkin, J. L., & Emery, W. J. (2005). Variability and forcing of the East Australian Current. *Journal of Geophysical Research*, *110*, C03019. hppts://doi.org/10.1029/2004JC002533

Brink, K. (2016). Cross-shelf exchange. *Annual Review of Marine Science*, *8*(1), 59–78. hppts://doi.org/10.1146/annurev-marine-010814-015717

Bull, C. Y., Kiss, A. E., Jourdain, N. C., England, M. H., & van Sebille, E. (2017). Wind forced variability in eddy formation, eddy shedding, and the separation of the East Australian Current. *Journal of Geophysical Research: Oceans*, *122*, 9980–9998. hppts://doi.org/10.1002/2017JC013311

Cetina-Heredia, P., Roughan, M., Liggins, G., Coleman, M. A., & Jeffs, A. (2019). Mesoscale circulation determines broad spatio-temporal settlement patterns of lobster. *PLoS ONE*, *14*(2), 1–20. hppts://doi.org/10.1371/journal.pone.0211722

Cetina-Heredia, P., Roughan, M., Sebille, E., Keating, S., & Brassington, G. B. (2019). Retention and leakage of water by mesoscale eddies in the East Australian Current system. *Journal of Geophysical Research: Oceans*, *124*, 2485–2500. hppts://doi.org/10.1029/2018JC014482

Cetina-Heredia, P., Roughan, M., van Sebille, E., & Coleman, M. A. (2014). Long-term trends in the East Australian Current separation latitude and eddy driven transport. *Journal of Geophysical Research: Oceans*, *119*, 4351–4366. hppts://doi.org/10.1002/2014JC010071

Chelton, D. B., Schlax, M. G., Samelson, R. M., & de Szoeke, R. A. (2007). Global observations of large oceanic eddies. *Geophysical Research Letters*, *34*, L15606. hppts://doi.org/10.1029/2007GL030812

Cotte, C., d'Ovidio, F., Chaigneau, A., Lévy, M., Taupier-Letage, I., Mate, B., & Guinet, C. (2011). Scale-dependent interactions of Mediterranean whales with marine dynamics. *Limnology and Oceanography*, *56*(1), 219–232. hppts://doi.org/10.4319/lo.2011.56.1.0219

Cresswell, G., & Legeckis, R. (1986). Eddies off southeastern Australia. *Deep Sea Research Part A. Oceanographic Research Papers*, *33*(11-12), 1527–1562. hppts://doi.org/10.1016/0198-0149(86)90066-X

d'Ovidio, F., Fernández, V., Hernández-García, E., & López, C. (2004). Mixing structures in the Mediterranean Sea from finite-size Lyapunov exponents. *Geophysical Research Letters*, *31*, L17203. hppts://doi.org/10.1029/2004GL020328

Dawson, A. (2016). EOFS: A library for EOF analysis of meteorological, oceanographic, and climate data. *Journal of Open Research Software*, *4*(1), e14. hppts://doi.org/10.5334/jors.122

Deng, X., Griffin, D. A., Ridgway, K., Church, J. A., Featherstone, W. E., White, N. J., & Cahill, M. (2011). Satellite altimetry for geodetic, oceanographic, and climate studies in the Australian region, *Coastal altimetry* (pp. 473–508). Berlin, Heidelberg: Springer Berlin Heidelberg. hppts://doi.org/10.1007/978-3-642-12796-0&urluscore;18

Everett, J. D., Baird, M. E., Oke, P. R., & Suthers, I. M. (2012). An avenue of eddies: Quantifying the biophysical properties of mesoscale eddies in the Tasman Sea. *Geophysical Research Letters*, *39*, L16608. hppts://doi.org/10.1029/2012GL053091

Everett, J. D., Baird, M. E., Roughan, M., Suthers, I. M., & Doblin, M. A. (2014). Relative impact of seasonal and oceanographic drivers on surface chlorophyll a along a Western Boundary Current. *Progress in Oceanography*, *120*, 340–351. hppts://doi.org/10.1016/j.pocean.2013.10.016

Everett, J. D., Macdonald, H., Baird, M. E., Humphries, J., Roughan, M., & Suthers, I. M. (2015). Cyclonic entrainment of preconditioned shelf waters into a frontal eddy. *Journal of Geophysical Research: Oceans*, *120*, 677–691. hppts://doi.org/10.1002/2014JC010301

Fewings, M., Lentz, S. J., Fredericks, J., Fewings, M., Lentz, S. J., & Fredericks, J. (2008). Observations of cross-shelf flow driven by cross-shelf winds on the inner continental shelf. *Journal of Physical Oceanography*, *38*(11), 2358–2378. hppts://doi.org/10.1175/2008JPO3990.1

Godfrey, J. S., Cresswell, G. R., Golding, T. J., Pearce, A. F., Boyd, R., Godfrey, J. S., et al. (1980). The separation of the East Australian Current. *Journal of Physical Oceanography*, *10*(3), 430–440. hppts://doi.org/10.1175/1520-0485(1980)010<0430:TSOTEA>2.0.CO;2

Gordon, A. L. (1989). Brazil-Malvinas Conlluence-1984. *Deep-Sea Research*, *36*(3), 359–384.

Harrison, C. S., & Siegel, D. A. (2014). The tattered curtain hypothesis revised: Coastal jets limit cross-shelf larval transport. *Limnology and Oceanography*, *4*, 50–66. hppts://doi.org/10.1215/21573689-2689820

He, R., Todd, A. C., Lembke, C., Kellison, T., Taylor, C., & Mann, D. A. (2018). Cross-shelf exchange associated with the Gulf Stream in the South Atlantic Bight: Direct observations using an autonomous underwater glider. *Marine Technology Society Journal*, *52*(3), 19–27.

Lutjeharms, J. (2006). *The Agulhas Current*, pp. 329: Springer.

Malan, N., Backeberg, B., Biastoch, A., Durgadoo, J. V., Samuelsen, A., Reason, C., & Hermes, J. (2018). Agulhas Current meanders facilitate shelf-slope exchange on the Eastern Agulhas Bank. *Journal of Geophysical Research: Oceans*, *123*, 4762–4778. hppts://doi.org/10.1029/2017JC013602

Mata, M. M., Wijffels, S. E., Church, J. A., & Tomczak, M. (2006). Eddy shedding and energy conversions in the East Australian Current. *Journal of Geophysical Research*, *111*, C09034. hppts://doi.org/10.1029/2006JC003592

Oke, P. R., Roughan, M., Cetina-Heredia, P., Pilo, G. S., Ridgway, K. R., Rykova, T., et al. (2019). Revisiting the circulation of the East Australian Current: Its path, separation, and eddy field. *Progress in Oceanography*, *176*, 102139. hppts://doi.org/10.1016/J.POCEAN.2019.102139

Oliver, E. C. J., O'Kane, T. J., & Holbrook, N. J. (2015). Projected changes to Tasman Sea eddies in a future climate. *Journal of Geophysical Research: Oceans*, *120*, 7150–7165. hppts://doi.org/10.1002/2015JC010993

Olson, D. B. (2001). Biophysical dynamics of western transition zones: A preliminary synthesis. *Fisheries Oceanography*, *10*(2), 133–150. hppts://doi.org/10.1046/j.1365-2419.2001.00161.x

Pallàs-Sanz, E., & Viúdez, Á. (2007). Three-dimensional ageostrophic motion in mesoscale vortex dipoles. *Journal of Physical Oceanography*, *37*(1), 84–105. hppts://doi.org/10.1175/JPO2978.1

Peterson, R. G., & Stramma, L. (1991). Upper-level circulation in the South Atlantic Ocean. *Progress in Oceanography*, *26*(1), 1–73. hppts://doi.org/10.1016/0079-6611(91)90006-8

Pilo, G. S., Mata, M. M., & Azevedo, J. L. L. (2015). Eddy surface properties and propagation at Southern Hemisphere western boundary current systems. *Ocean Science*, *11*, 629–641. hppts://doi.org/10.5194/os-11-629-2015

Pilo, G. S., Oke, P. R., Coleman, R., Rykova, T., & Ridgway, K. (2018). Patterns of vertical velocity induced by eddy distortion in an ocean model. *Journal of Geophysical Research: Oceans*, *123*, 2274–2292. hppts://doi.org/10.1002/2017JC013298

Ribbe, J., & Brieva, D. (2016). A western boundary current eddy characterisation study. *Estuarine, Coastal and Shelf Science*, *183*, 203–212. hppts://doi.org/10.1016/j.ecss.2016.10.036

Ridgway, K. R., Dunn, J. R., Wilkin, J. L., Ridgway, K. R., Dunn, J. R., & Wilkin, J. L. (2002). Ocean interpolation by four-dimensional weighted least squares: Application to the waters around Australasia. *Journal of Atmospheric and Oceanic Technology*, *19*(9), 1357–1375. hppts://doi.org/10.1175/1520-0426(2002)019<1357:OIBFDW>2.0.CO;2

Roughan, M., Keating, S. R., Schaeffer, A., Cetina-Heredia, P., Rocha, C., Griffin, D., et al. (2017). A tale of two eddies: The biophysical characteristics of two contrasting cyclonic eddies in the East Australia Current System. *Journal of Geophysical Research: Oceans*, *122*, 2494–2518. hppts://doi.org/10.1002/2016JC012241

Roughan, M., Macdonald, H. S., Baird, M. E., & Glasby, T. M. (2011). Modelling coastal connectivity in a Western Boundary Current: Seasonal and inter-annual variability. *Deep Sea Research Part II: Topical Studies in Oceanography*, *58*(5), 628–644. hppts://doi.org/10.1016/J.DSR2.2010.06.004

Roughan, M., Oke, P. R., Middleton, J. H., Roughan, M., Oke, P. R., & Middleton, J. H. (2003). A modeling study of the climatological current field and the trajectories of upwelled particles in the East Australian Current. *Journal of Physical Oceanography*, *33*(12), 2551–2564. hppts://doi.org/10.1175/1520-0485(2003)033<2551:AMSOTC>2.0.CO;2

Ryan, J. P., Yoder, J. A., Barth, J. A., & Cornillon, P. C. (1999). Chlorophyll enhancement and mixing associated with meanders of the shelf break front in the Mid-Atlantic Bight. *Journal of Geophysical Research*, *104*(C10), 23,479–23,493. hppts://doi.org/10.1029/1999JC900174

Rykova, T., & Oke, P. R. (2015). Recent freshening of the East Australian Current and its eddies. *Geophysical Research Letters*, *42*, 9369–9378. hppts://doi.org/10.1002/2015GL066050

Rykova, T., Oke, P. R., & Griffin, D. A. (2017). A comparison of the structure, properties, and water mass composition of quasi-isotropic eddies in western boundary currents in an eddy-resolving ocean model. *Ocean Modelling*, *114*, 1–13. hppts://doi.org/10.1016/j.ocemod.2017.03.013

Schaeffer, A., Gramoulle, A., Roughan, M., & Mantovanelli, A. (2017). Characterizing frontal eddies along the East Australian Current from HF radar observations. *Journal of Geophysical Research: Oceans*, *122*, 3964–3980. hppts://doi.org/10.1002/2016JC012171

Schaeffer, A., Roughan, M., & Morris, B. D. (2013). Cross-shelf dynamics in a western boundary current regime: Implications for upwelling. *Journal of Physical Oceanography*, *43*(5), 1042–1059. hppts://doi.org/10.1175/JPO-D-12-0177.1

Schaeffer, A., Roughan, M., & Wood, J. E. (2014). Observed bottom boundary layer transport and uplift on the continental shelf adjacent to a western boundary current. *Journal of Geophysical Research: Oceans*, *119*, 4922–4939. hppts://doi.org/10.1002/2013JC009735

Sloyan, B. M., Ridgway, K. R., Cowley, R., Sloyan, B. M., Ridgway, K. R., & Cowley, R. (2016). The East Australian Current and property transport at 27°S from 2012 to 2013. *Journal of Physical Oceanography*, *46*(3), 993–1008. hppts://doi.org/10.1175/JPO-D-15-0052.1

Tomczak, M., & Godfrey, J. S. (2003). *Regional oceanography: An introduction*. New Delhi, India: Daya Publishing House.

Vélez-Belchí, P., Centurioni, L. R., Lee, D.-K., Jan, S., & Niiler, P. P. (2013). Eddy induced Kuroshio intrusions onto the continental shelf of the East China Sea. *Journal of Marine Research*, *71*(1), 83–107. hppts://doi.org/10.1357/002224013807343470

Wu, L., Cai, W., Zhang, L., Nakamura, H., Timmermann, A., Joyce, T., et al. (2012). Enhanced warming over the global subtropical western boundary currents. *Nature Climate Change*, *2*(3), 161–166. hppts://doi.org/10.1038/nclimate1353

Zhang, W. G., & Gawarkiewicz, G. G. (2015). Dynamics of the direct intrusion of Gulf Stream ring water onto the Mid-Atlantic Bight shelf. *Geophysical Research Letters*, *42*, 7687–7695. hppts://doi.org/10.1002/2015GL065530

Zhang, Z., Qiu, B., Klein, P., & Travis, S. (2019). The influence of geostrophic strain on oceanic ageostrophic motion and surface chlorophyll. *Nature Communications*, *10*(1), 2838. hppts://doi.org/10.1038/s41467-019-10883-w